Noname manuscript No.
(will be inserted by the editor)

Supplementary Information

Insights into the elevation-dependent warming in the Tibetan Plateau-Himalayas from CMIP5 model simulations

Elisa Palazzi · Luca Filippi · Jost von Hardenberg

Received: date / Accepted: date

1 Assessment of the individual CMIP5 model outputs

This section analyses how the individual CMIP5 models reproduce elevation-dependent warming (EDW) in the Tibetan Plateau-Himalayas (70°E-105°E, 25°N-40°N) and discusses more in detail the statistics of GCM ensemble and the inter-model spread.

1.1 Historical period: 1871–2000

Table S1 shows, for each GCM, the slope of the linear regression (°C km^{-1}) describing the 20$^{\text{th}}$ century changes (1971–2000 climatology minus 1871–1900 climatology) of minimum temperatures as a function of the surface elevation for each season in the Tibetan Plateau-Himalayan region. Each model is analyzed at its native spatial resolution shown in Table 1 of the main paper. For completeness, values of the MMM, are also reported. Stars in parentheses indicate statistically significant ($p < 0.05$) elevational gradients of warming rates, the significance being assessed through the Monte Carlo "shuffling" method described in the methodological section of the paper. Most of the models show statistically significant elevational gradients of the minimum temperature changes. For most of them (67% in winter, 70% in spring and 65% in

E. Palazzi
Institute of Atmospheric Sciences and Climate, National Research Council (ISAC-CNR), corso Fiume 4, 10133, Torino, Italy
Tel.: +39-011-3839834
Fax: +39-011-6600364
E-mail: e.palazzi@isac.cnr.it

L. Filippi
Institute of Atmospheric Sciences and Climate, National Research Council (ISAC-CNR)

J. von Hardenberg
Institute of Atmospheric Sciences and Climate, National Research Council (ISAC-CNR)

autumn) the slopes are positive denoting higher warming rates as the altitude increases. During summer 55% of the models indicate a negative slope instead (i.e., reduced warming rate with the elevation), even if the slope of the MMM is positive. Table S2 shows the same as Table S1, but for the maximum temperature. In this case 67% of the models showing statistically significant elevational gradients during winter have a positive slope; the percentage during spring is 69%, in summer it is 65%, and it is 61% in autumn. Therefore, while the MMM indicates statistically significant warming trends with elevation, for both minimum and maximum temperatures and in all seasons, there are noticeable inter-model differences, such that some models agree very well with the MMM but others may even exhibit slopes of opposite sign. The

Table S1 Slope of linear regressions (°C km^{-1}) describing the elevational gradients of the minimum temperature changes between the 1971–2000 climatology and the 1871–1900 climatology for each season in the Tibetan Plateau-Himalayan region and for each CMIP5 model. Stars in parentheses indicate statistically significant slopes ($p < 0.05$). The table also shows the slope of the linear regression and its significance for the CMIP5 multi-model mean (MMM) calculated after regridding each model into a 2×2 degrees horizontal grid.

Model ID	DJF	MAM	JJA	SON
CCSM4	0.0725(∗)	0.0770(∗)	−0.0323(∗)	0.0809(∗)
CESM1-BGC	−0.0618(∗)	0.0059	−0.0226(∗)	0.0421(∗)
CESM1-CAM5	0.0464(∗)	0.0909(∗)	0.2278(∗)	0.0843(∗)
bcc-csm1-1-m	0.1649(∗)	0.0287(∗)	−0.0346(∗)	0.0618(∗)
MRI-CGCM3	−0.1008(∗)	−0.0448(∗)	−0.0438(∗)	−0.0285(∗)
CNRM-CM5	0.0610(∗)	0.0726(∗)	−0.0442(∗)	0.1205(∗)
MIROC5	0.0383(∗)	0.0491(∗)	−0.0855(∗)	0.0658(∗)
ACCESS1-0	0.0626(∗)	0.0053	−0.0158(∗)	−0.0016
ACCESS1-3	−0.0758(∗)	−0.0252(∗)	−0.0026	−0.0927(∗)
HadGEM2-CC	−0.1832(∗)	−0.0843(∗)	0.1542(∗)	0.1871(∗)
IPSL-CM5A-MR	0.1883(∗)	0.2250(∗)	0.2368(∗)	0.1867(∗)
INM-CM4	0.0157	0.2423(∗)	0.0967(∗)	0.1797(∗)
CSIRO-Mk3-6-0	0.1022(∗)	0.1013(∗)	−0.0145	−0.0218(∗)
NorESM1-M	0.0228	0.0458(∗)	−0.0177	−0.0540(∗)
GFDL-CM3	0.0208	−0.0154	−0.0602(∗)	0.0191
GFDL-ESM2G	0.0162	−0.0973(∗)	0.0132	−0.1478(∗)
GFDL-ESM2M	0.0874(∗)	−0.0132	0.0187	0.0562(∗)
GISS-E2-H	−0.1519(∗)	−0.1212(∗)	−0.1755(∗)	−0.0869(∗)
GISS-E2-R	0.0174	−0.0401	0.0429(∗)	0.0958(∗)
IPSL-CM5A-LR	0.0216	0.1572(∗)	0.2619(∗)	0.0696
IPSL-CM5B-LR	0.0643	0.0366	0.0878(∗)	0.0108
MIROC-ESM-CHEM	0.1034(∗)	0.2060(∗)	−0.0125	0.2179(∗)
MIROC-ESM	0.1634(∗)	0.2742(∗)	−0.0713	0.2292(∗)
bcc-csm1-1	0.0516	0.0567(∗)	−0.0326(∗)	−0.1093(∗)
BNU-ESM	−0.0253	0.009	0.1730(∗)	0.1528(∗)
CanESM2	−0.2605(∗)	−0.0727(∗)	−0.0791(∗)	−0.0966(∗)
FGOALS-g2	0.1469(∗)	0.1083(∗)	0.0354(∗)	0.0843(∗)
MMM	0.0135(∗)	0.0348(∗)	0.0106(∗)	0.0173(∗)

values shown in Tables S1 and SS2 thus suggest that the inter-model variabil-

Table S2 The same as Table S1 but for the maximum temperature.

Model ID	DJF	MAM	JJA	SON
CCSM4	0.0923(∗)	0.0742	0.0050(∗)	0.1051(∗)
CESM1-BGC	0.0061	−0.0161	0.1071(∗)	0.0630(∗)
CESM1-CAM5	0.1523(∗)	0.1201(∗)	0.2443(∗)	0.0672(∗)
bcc-csm1-1-m	0.1570(∗)	0.0162(∗)	0.0434(∗)	0.0483(∗)
MRI-CGCM3	0.0236(∗)	0.0251(∗)	−0.0395(∗)	−0.0051
CNRM-CM5	−0.0281(∗)	−0.0151	−0.0715(∗)	0.0667(∗)
MIROC5	0.0321(∗)	0.0488(∗)	−0.0563(∗)	0.0113
ACCESS1-0	0.1117(∗)	−0.0228	−0.0022	0.0118
ACCESS1-3	−0.0491(∗)	−0.0659(∗)	0.0289(∗)	−0.1185(∗)
HadGEM2-CC	−0.3635(∗)	−0.3967(∗)	−0.1294(∗)	−0.1774(∗)
IPSL-CM5A-MR	0.1887(∗)	0.2745(∗)	0.1049(∗)	0.0653(∗)
INM-CM4	0.2734	0.0439	0.0314	0.1488
CSIRO-Mk3-6-0	0.0987(∗)	0.0609(∗)	−0.0201(∗)	0.0308(∗)
NorESM1-M	0.0612(∗)	0.0719(∗)	−0.0247	−0.0721(∗)
GFDL-CM3	0.1184(∗)	0.1070(∗)	−0.0184	0.0896(∗)
GFDL-ESM2G	0.0401	0.0111	0.0008	−0.2052(∗)
GFDL-ESM2M	0.1171(∗)	−0.0466(∗)	−0.0470	0.0384
GISS-E2-H	−0.0776(∗)	−0.0102	0.0543	0.0770(∗)
GISS-E2-R	0.0123	−0.0026	0.0579(∗)	0.0113
IPSL-CM5A-LR	0.0043	0.1164(∗)	0.1816(∗)	0.0929(∗)
IPSL-CM5B-LR	0.0259	0.0059	0.0851(∗)	−0.0208
MIROC-ESM-CHEM	−0.0191	0.2179(∗)	−0.0155	0.1213
MIROC-ESM	−0.0091	0.2574(∗)	−0.1692	0.1716(∗)
bcc-csm1-1	0.0071	−0.0551(∗)	0.0563(∗)	−0.1421(∗)
BNU-ESM	−0.0253(∗)	0.009	0.1730(∗)	0.1528(∗)
CanESM2	−0.2370(∗)	−0.2007(∗)	−0.1648(∗)	−0.1025(∗)
FGOALS-g2	0.0426(∗)	−0.0354	0.0097	0.0051
MMM	0.0262(∗)	0.0165(∗)	0.0154(∗)	0.0164(∗)

ity around the MMM is high. This spread is displayed in Fig. S1 which shows the historical change (1971–2000 climatology minus 1871–1900 climatology) in minimum temperature (left panels) and in maximum temperature (right panels) as a function of the surface elevation in the CMIP5 ensemble for the four seasons. Elevational bins of 150-m thickness have been considered in which the following statistics of the GCM ensemble are calculated: the MMM (black line) and multi-model median (red line), the 25^{th} and 75^{th} percentiles (dashed red lines), the range of model variability (grey shading) which is expressed as one standard deviation above and below the mean – a quantitative measure of the inter-model spread (IMS). The statistics are reported provided that the number of contributing GCMs is greater than 10, a condition which is not verified for the last four bins (5,400–5,550 m, 5,550–5,700 m, 5,700–5,850 m, 5,850–6,000 m).

As also shown in Fig. S2, IMS tends to increase as the elevation increases, particularly from ∼3,000 m above sea level upward. In regards to that, it is worth noting that the number of models contributing to the statistics in the various bins varies from a minimum of 19 (corresponding to the altitudinal bin

975-1,275 m above sea level) to a maximum of 27, found in the bins centered around the following altitudes: 1,575 m, 2,025 m, 2,325 m, 2,625 m, 2,925 m, 3,225 m, 3,375 m, 3,525 m, 3,675 m, 4,575 m, 4,725 m. For minimum temperature (Fig. S2, left), in spite of the dependence of the inter-model spread on the elevation, the highest IMS values are found in winter (black line) across almost all the altitudinal belts, while the IMS values in the other seasons are more similar across the various bins. For maximum temperature (right panel of Fig. S2) there are no noticeable differences in the IMS values and in their dependence on the elevation from season to season, except that from about 4,500 m above sea level upward, where the IMS values in winter and spring are higher than in summer and autumn.

1.2 Projected changes: 1971–2100

Tables S3 and S4 show the same as Tables S1 and S2 but for the scenario simulations. The temperature changes have been evaluated between the 2071-2100 climatology and the 1971–2000 climatology, using the output of the model projections under the RCP 8.5 emission scenario from 2006 onward. In this case, there are many more models that show positive slopes of either the minimum and maximum temperature change with the elevation with respect to the historical model simulations. Almost 90% of the models for which the slopes are statistically significant indicate positive elevational gradients of the minimum temperature change in all seasons. For the maximum temperature change, this situation is even amplified: in autumn, all models give rise to statistically significant elevational gradients and all of them are positive; the percentage of models giving rise to statistically significant positive slopes is very high also in the other seasons (95% in winter, 88% in spring, 96% in summer). However, the inter-model spread in the scenario simulations remains very high , even larger than for the historical simulations. This can be noticed also in Fig. S3 (analogous to Fig. S1) for the scenario simulations. Despite the fact that most slopes are positive in the projections indicating more coherence among the models in the sign of the elevational gradients of warming trends with respect to the historical simulations, the inter-model spread is large and it increases with the elevation (see also Fig. S4) . For minimum temperatures in particular we observe larger values of IMS in winter and in spring than in the other seasons between about 3,500 and 4,200 m above sea level.

As already discussed in the main paper, both Figs. S1 and S3 suggest that a differential level of warming occurs below and above about 1,500-2,000 m above sea level.

2 Further considerations on the EDW in the historical period: models and observations

Figure S5 shows the minimum (blue) and maximum (red) temperature changes in the historical period (between the 1971–2000 climatology and the 1871–

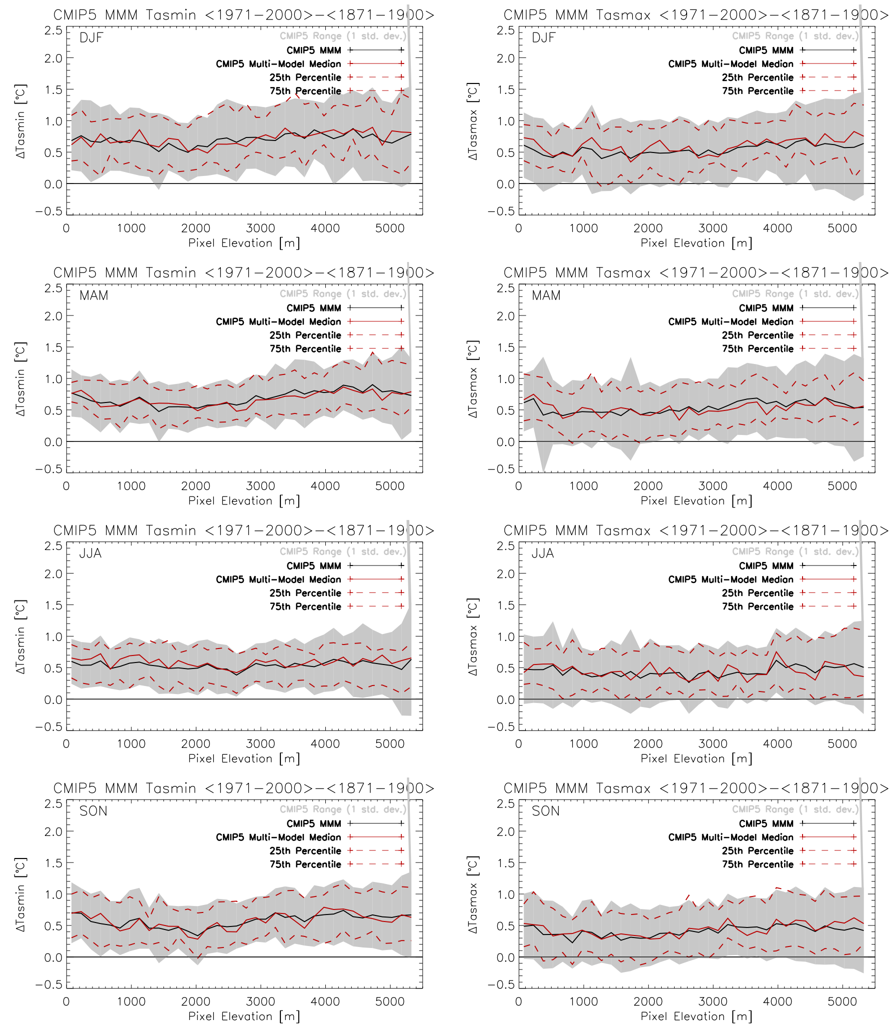

Fig. S1 Statistics of the historical change (1971–2000 climatology minus 1871–1900 climatology, in °C) in the minimum temperature (left panels) and in the maximum temperature (right panels) as a function of surface elevation (150 m-thick bins) in the CMIP5 ensemble for the four seasons. The CMIP5 MMM and multi-model median are shown with the solid black and red line, respectively; the 25^{th} and 75^{th} percentiles are represented by dashed red lines while the range of variability (expressed as one standard deviation) is the grey area).

1900 climatology) for the CMIP5 model ensemble as a function of the mean temperature. Superimposed are the minimum (black) and maximum (yellow) temperature changes (1971–2000 climatology minus 1901–1930 climatology) as a function of the mean temperature for observations taken from the University of East Anglia Climate Research Unit (CRU) temperature dataset, version TS3.22. The gridded CRU TS3.22 data provide month-by-month vari-

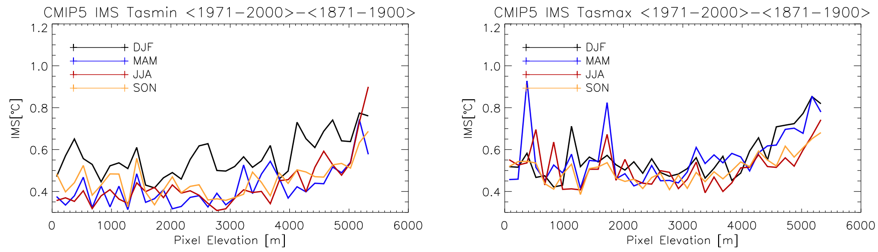

Fig. S2 Standard deviation of the historical change (1971–2000 climatology minus 1871–1900 climatology, in °C) in minimum temperatures (left panels) and in maximum temperatures (right panels) as a function of surface elevation (150 m-thick bins) in the CMIP5 ensemble for the four seasons.

ations of, among other variables, the minimum and maximum temperature over the period 1901-2013, on high-resolution (0.5×0.5 degree) grids (CRU, 2014). The line-filled (solid-filled) areas represent the range of variability of the models measured as one standard deviation above and below the MMM for the minimum temperature (maximum temperature).

Despite differences in the absolute values of the change (please note that the temperature change is calculated between the climatology of different time periods in the observations and in the model simulations), there is a qualitative agreement between CRU and the CMIP5 MMM, especially in winter. The relationship between the temperature changes and the elevation is in fact similarly reproduced in the observations and in the CMIP5 models, in spite of the very pronounced peak around −5°C seen in CRU, corresponding to altitudes around 1,000 m above sea level. However, it is worth pointing out that a comparative analysis between the models and the CRU gridded observations is hampered by the scarcity of observational data in this region, which introduces a large amount of uncertainties in the CRU dataset which is based on the interpolation of station data. With regards to that, the left panel of Fig. S6 shows the monthly time series, from 1901 to 2013, of the total number of stations in the entire study area (see Figure 1 of the main text). The right panel shows the spatial distribution of the maximum number of stations in the area. This figure shows, in a very clear way, that the CRU dataset, as well as many other gridded observational datasets that are available for this region, should be regarded with caution since the sparsity of the underlying in-situ stations constitutes a great source of uncertainty in the final product (see also Palazzi et al, 2013, which analyzed this issue for the gridded precipitation datasets in the Karakoram-Himalaya region). Most studies which already analyzed the EDW in the Tibetan Plateau region from observations used the data collected by in-situ meteorological stations managed by different agencies indeed, rather than interpolated datasets.

Table S3 Slope of linear regressions (°C km^{-1}) describing 21st century changes (2071–2100 climatology minus 1971–2000 climatology) in minimum temperatures as a function of surface elevation for each season in the Tibetan Plateau-Himalayan region and for each CMIP5 model. Stars in parentheses indicate statistically significant trends of the temperature changes with elevation ($p < 0.05$). The table also show the slope of the linear regression and its significance for the CMIP5 multi-model mean (MMM) calculated after regridding each model into a 2×2 degrees horizontal grid.

Model ID	DJF	MAM	JJA	SON
CCSM4	0.2877(∗)	0.2522(∗)	0.1173(∗)	0.4709(∗)
CESM1-BGC	0.3746(∗)	0.2861(∗)	0.1395(∗)	0.5024(∗)
CESM1-CAM5	0.2215(∗)	0.2969(∗)	0.1856(∗)	0.5270(∗)
bcc-csm1-1-m	0.0666(∗)	0.3218(∗)	0.0215	0.2655(∗)
MRI-CGCM3	0.2180(∗)	0.2963(∗)	−0.1597(∗)	0.1996(∗)
CNRM-CM5	0.0845(∗)	0.0725(∗)	0.3768(∗)	0.3715(∗)
MIROC5	0.5820(∗)	0.6507(∗)	0.7439(∗)	0.6464(∗)
ACCESS1-0	0.5868(∗)	0.3837(∗)	0.1200(∗)	0.3559(∗)
ACCESS1-3	0.0634	−0.1024(∗)	0.0262	−0.1568(∗)
HadGEM2-CC	0.4784(∗)	0.1657(∗)	−0.0205	−0.0667
IPSL-CM5A-MR	0.5710(∗)	0.9932(∗)	0.7807(∗)	0.7555(∗)
INM-CM4	0.4045(∗)	0.3555(∗)	0.2390(∗)	0.0788
CSIRO-Mk3-6-0	−0.1364(∗)	−0.0168	−0.3181(∗)	−0.2246(∗)
NorESM1-M	0.0228	0.1197(∗)	0.1292(∗)	0.4294(∗)
GFDL-CM3	0.8013(∗)	0.2334(∗)	0.4409(∗)	0.0311
GFDL-ESM2G	0.2719(∗)	−0.0862	0.0591	0.596
GFDL-ESM2M	0.1237	−0.1202(∗)	−0.0986	−0.1100
GISS-E2-H	0.2650(∗)	0.2967(∗)	0.4443(∗)	0.2420(∗)
GISS-E2-R	0.2810(∗)	0.3123(∗)	0.3612(∗)	0.2227(∗)
IPSL-CM5A-LR	0.7722(∗)	0.9205(∗)	0.6992(∗)	0.7080(∗)
IPSL-CM5B-LR	−0.3270(∗)	−0.1847	0.0073	−0.1412
MIROC-ESM-CHEM	1.0942(∗)	0.9205(∗)	0.9234(∗)	0.8005(∗)
MIROC-ESM	1.0143(∗)	0.6984(∗)	1.0271(∗)	0.9246(∗)
bcc-csm1-1	0.4102(∗)	0.0613	−0.07234	0.0260
BNU-ESM	0.3852(∗)	0.2155(∗)	0.0021	0.2584(∗)
CanESM2	0.1108	0.3518(∗)	0.3253(∗)	0.0294
FGOALS-g2	0.3648(∗)	0.4250(∗)	0.6463(∗)	0.5142(∗)
MMM	0.3701(∗)	0.2803(∗)	0.2807(∗)	0.2789(∗)

References

CRU (University of East Anglia Climatic Research Unit): Ian Harris, Phil Jones: CRU TS3.22: Climatic Research Unit (CRU) Time-Series (TS) Version 3.22 of High Resolution Gridded Data of Month-by-month Variation in Climate (Jan. 1901- Dec. 2013). NCAS British Atmospheric Data Centre, 24 September 2014 , DOI 10.5285/18BE23F8-D252-482D-8AF9-5D6A2D40990C, `http://dx.doi.org/10.5285/18BE23F8-D252-482D-8AF9-5D6A2D40990C` (2014)

Palazzi E, von Hardenberg J, Provenzale A, Precipitation in the Hindu-Kush Karakoram Himalaya: Observations and future scenarios, J. Geophys. Res., 118:85–100, DOI 10.1029/2012JD018697 (2013)

Table S4 The same as Table S3 but for the maximum temperature.

Model ID	DJF	MAM	JJA	SON
CCSM4	0.1597(∗)	0.0256	0.1539(∗)	0.2769(∗)
CESM1-BGC	0.1860(∗)	0.1271(∗)	0.1808(∗)	0.2977(∗)
CESM1-CAM5	0.1345(∗)	0.1350(∗)	0.1658(∗)	0.3480(∗)
bcc-csm1-1-m	−0.0084	0.0280	0.3870(∗)	0.3276(∗)
MRI-CGCM3	0.2194(∗)	0.0436(∗)	−0.0833(∗)	0.1220(∗)
CNRM-CM5	0.0098	−0.0736(∗)	0.2748(∗)	0.3410(∗)
MIROC5	0.2943(∗)	0.3857(∗)	0.7418(∗)	0.7996(∗)
ACCESS1-0	0.3555(∗)	0.1849(∗)	0.0637	0.3403(∗)
ACCESS1-3	0.1934(∗)	0.0848(∗)	0.2664(∗)	0.2096(∗)
HadGEM2-CC	0.6138(∗)	0.3117(∗)	0.2235(∗)	0.5364(∗)
IPSL-CM5A-MR	0.3869(∗)	0.7101(∗)	0.0371	0.4038(∗)
INM-CM4	0.3845(∗)	0.5113(∗)	0.2300(∗)	0.3486(∗)
CSIRO-Mk3-6-0	0.0280	0.1143(∗)	0.1264(∗)	0.1791(∗)
NorESM1-M	−0.0225	0.0565	0.3158(∗)	0.3865(∗)
GFDL-CM3	1.1250(∗)	0.5482(∗)	0.8839(∗)	1.2325(∗)
GFDL-ESM2G	0.3624(∗)	0.0249	0.2318(∗)	0.4521(∗)
GFDL-ESM2M	0.2881(∗)	0.0448	0.0754	0.1881(∗)
GISS-E2-H	0.1846(∗)	0.3817(∗)	0.8583(∗)	0.3958(∗)
GISS-E2-R	0.3205(∗)	0.4212(∗)	0.8243(∗)	0.4876(∗)
IPSL-CM5A-LR	0.3232(∗)	0.5499(∗)	−0.0393	0.2591(∗)
IPSL-CM5B-LR	0.0066	0.0538	0.0918(∗)	0.1669(∗)
MIROC-ESM-CHEM	0.4030(∗)	0.1926	0.8054(∗)	0.7354(∗)
MIROC-ESM	0.3789(∗)	0.0925	1.001(∗)	0.8286(∗)
bcc-csm1-1	−0.0040	−0.2446(∗)	0.3642(∗)	0.2016(∗)
BNU-ESM	−0.1067	0.3215(∗)	0.3774(∗)	0.5989(∗)
CanESM2	0.1286(∗)	0.1668	0.6585(∗)	0.1568(∗)
FGOALS-g2	−0.2748(∗)	−0.1021	1.0018(∗)	0.2257(∗)
MMM	0.2635(∗)	0.2231(∗)	0.3816(∗)	0.4584(∗)

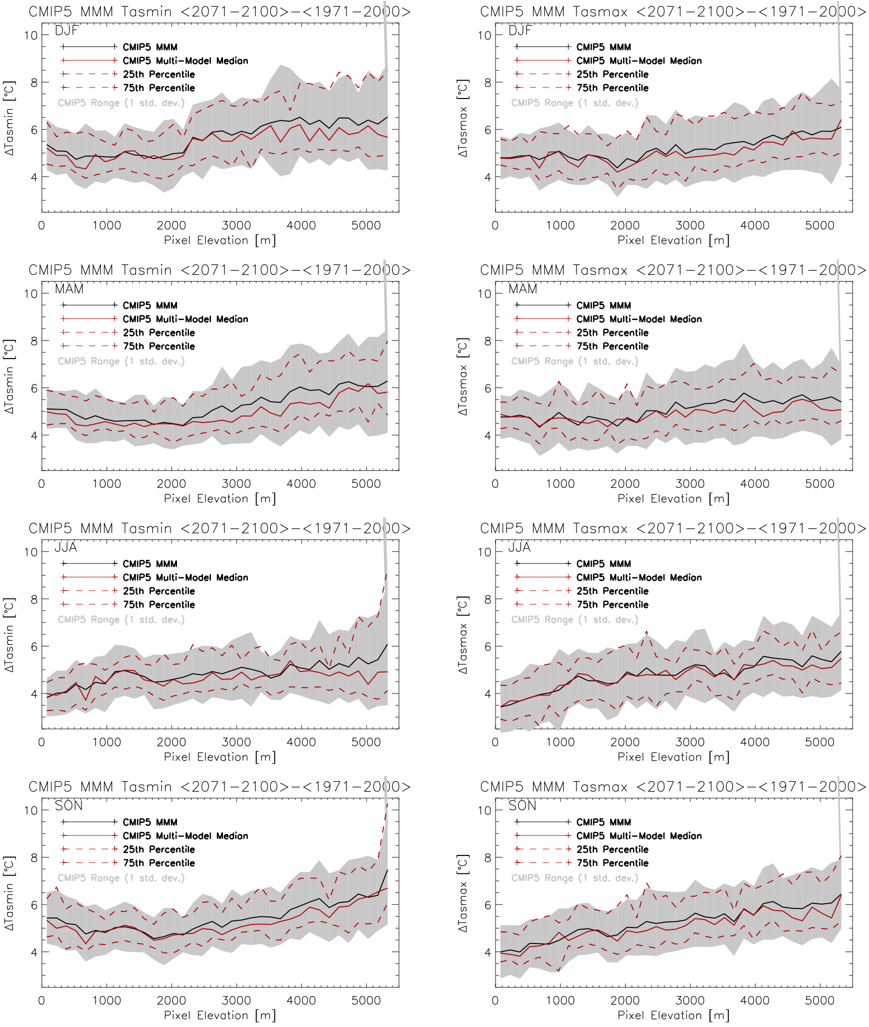

Fig. S3 Statistics of the future change (2071–2100 climatology minus 1971–2000 climatology, in °C)) in minimum temperatures (left panels) and in maximum temperatures (right panels) as a function of surface elevation (150 m-thick bins) in the CMIP5 ensemble for the four seasons. The CMIP5 MMM and multi-model median are shown with the solid black and red line, respectively; the 25th and 75th percentiles are represented by dashed red lines while the range of variability (expressed as one standard deviation) is the grey area).

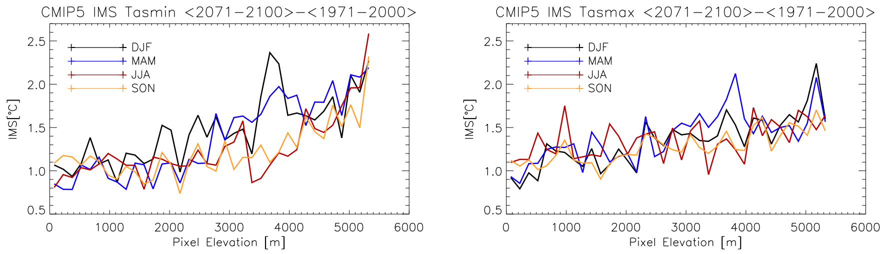

Fig. S4 Standard deviation of the historical change (2071–2100 climatology minus 1971–2000 climatology, in °C) in minimum temperatures (left panels) and in maximum temperatures (right panels) as a function of surface elevation (150 m-thick bins) in the CMIP5 ensemble for the four seasons.

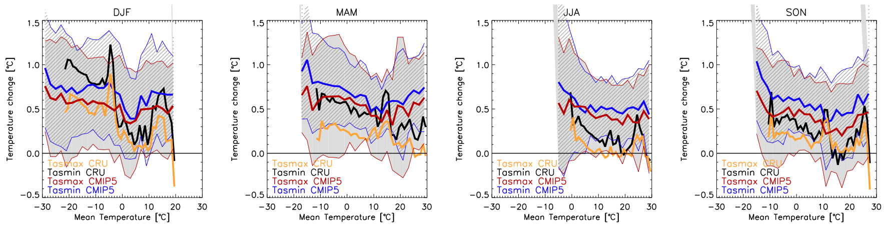

Fig. S5 Minimum and maximum temperature change between the 1971–2000 climatology and the 1871–1900 climatology as a function of surface elevation for the multi model mean data averaged in 150 m-thick bins (top panels) and as a function of the mean temperature for the multi model mean data averaged in 1°C-thick bins for the four seasons (middle panels). The blue (red) lines show the multi model mean of the GCM ensemble while the grey (light grey) shaded areas represent the range of variability of the models measured as one standard deviation above and below the MMM for minimum temperatures (maximum temperatures). In the bottom panels the minimum and maximum temperature change between the 1971–2000 climatology and the 1901–1930 climatology as a function of surface elevation for the CRU data averaged in 150 m-thick bins is also shown together with the CMIP5 MMM.

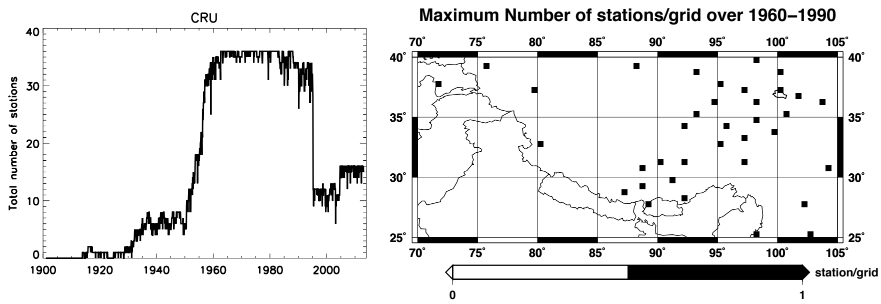

Fig. S6 (Left) Monthly time series of the number of stations in the study area for the CRU dataset for the period 1901–2013. (Right) Spatial distribution of the maximum number of in-situ stations per grid in the study area.